Robust control of synchronous motors through AC/DC/AC converters

Abdelmounime El Magri, Fouad Giri, Abdelmajid Abouloifa, Fatima Zara Chaoui

Robust control of synchronous motor through AC/DC/AC converters

A. El Magri, F. Giri *, A. Abouloifa, F.Z. Chaoui

GREYC Lab, University of Caen, 14032 Caen, France

Keywords:
Synchronous motor
DC–AC inverter
Nonlinear control
Power factor correction
Parameter uncertainty
Average analysis

A B S T R A C T

The problem of controlling synchronous motors, driven through AC/DC rectifiers and DC/AC inverters is addressed. The control objectives are threefold: (i) forcing the motor speed to track a varying reference signal in presence of motor parameter uncertainties; (ii) regulating the DC Link voltage; (iii) assuring a satisfactory power factor correction (PFC) with respect to the power supply net. First, a nonlinear model of the whole controlled system is developed in the Park-coordinates. Then, a robust nonlinear controller is synthesized using the damping function version of the backstepping design technique. A formal analysis based on Lyapunov stability and average theory is developed to describe the control system performances. Despite parameter uncertainties, all control objectives are proved to be asymptotically achieved up to unavoidable but small harmonic errors (ripples).

1. Introduction

Permanent magnet synchronous (PMS) motors are more suitable (compared e.g. to induction motors) for electric traction and other applications. Indeed, they possess a better mass/power ratio, develop a much higher power level and present a more satisfactory efficiency. These benefits come from the fact that Joule losses in PMS motors are much less important as no field or rotor currents are involved. A considerable progress has been made in power electronics technology leading to reliable power electronic converters and making possible varying speed drive of synchronous machines. Indeed, speed variation can only be achieved for these machines by acting on the supply net frequency. Until the development of modern power electronics, there was no effective and simple way to vary the frequency of a supply net. On the other hand, in the electric traction domain, the used power nets are either DC or AC but mono-phase. Therefore, three-phase DC/AC inverters turn out to be the only possible interface (between the main power supply nets and 3-phase AC motors) due to their high capability to ensure flexible voltage and frequency variation. The above considerations illustrate the major role of modern power electronics in the recent development of electrical traction applications (locomotives, vehicles, etc.). As mentioned above, a three-phase DC/AC inverter used in traction is supplied by a power net that can be either DC or mono-phase AC. In the case of AC supply, the (mono-phase) net is connected to the three-phase DC/AC inverter through a transformer and an AC/DC rectifier (Fig. 1). The connection line between the rectifier and the inverter is called DC link.

The control problem at hand is to design a controller ensuring a wide speed range regulation for the system including the AC/DC converter, the DC/AC inverter and the PMS motor. The point is that such system behaves as a nonlinear load vis-à-vis to the AC supply line. Then, undesirable current harmonics are likely to be generated in the AC line. These harmonics reduce the rectifier efficiency, induce voltage distortion in the AC supply line and cause electromagnetic compatibility problems. The pollution caused by the converter may be reduced resorting to additional protection equipments (transformers, condensers, etc.) and/or over-dimensioning the converter and net elements. However, this solution is costly and may not be sufficient. To overcome this drawback, the control objective must not only be motor speed regulation but also current harmonics rejection. The last objective is referred to power factor correction (PFC) (Singh, Bhuvaneswari, & Garg, 2006).

Most previous works on synchronous machine speed control have simplified the control problem neglecting the dynamics of the AC/DC rectifier, i.e. focusing only on the set 'DC/AC inverter-motor'. This reduced system has been dealt with using several control strategies ranging from simple techniques, e.g. field-oriented control (Saleh, Mohammed, & Badr, 2004), to more sophisticated nonlinear approaches, e.g. feedback linearization (Kuroe, Okamura, Nishidai, & Maruhashi, 1998), direct torque control (Pyrhonen, Niemela, Pyrhonen, & Kaukonen, 1998), sliding mode (Yang, Wang, Liu, Hou, & Cai, 1992), hybrid sliding-mode/neurofuzzy control (Elmas & Ustun, 2008). A control strategy that ignores the presence of the AC/DC rectifier suffers at least from two drawbacks. First, the controller design relies on the

* Corresponding author.
E-mail address: fouad.giri@unicaen.fr (F. Giri).

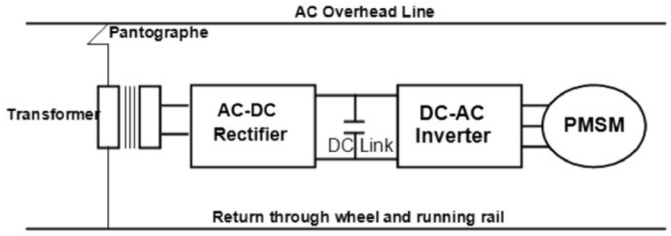

Fig.1. Schematic representation of single phase AC supply powering 3-phase AC motor.

assumption that the DC voltage (provided by the AC/DC rectifier) is perfectly regulated; the point is that perfect regulation of the rectifier output voltage cannot be ensured ignoring the rectifier load, which is nothing other than the set 'DC/AC inverter-motor'. The second drawback lies in the entire negligence of the PFC requirement. That is, from a control viewpoint, it is not judicious to consider separately the inverter-motor association, on one hand, and the power rectifier, on the other hand.

In the present work, a new control strategy is developed that simultaneously deals with both involved subsystems, i.e. the AC/DC inverter and the combination 'DC/AC inverter-motor'. The new control strategy is featured by its multi-loops nature and its robustness against parametric uncertainty. First, a current loop is designed so that the coupling between the power supply net and the AC/DC rectifier operates with a unitary power factor. Then, a second loop is designed to regulate the output voltage of the AC/DC rectifier so that the DC-link between the rectifier and the inverter operates with a constant voltage despite changes of the motor operation conditions. Finally, a bi-variable regulator is constructed to make the motor velocity track its varying reference value and to regulate the *d*-component of stator current to zero optimizing thus the absorbed stator current. The bi-variable regulator is designed using the damping function version of the backstepping technique (Krstic, Kanellakopoulos, & Kokotovic, 1995). Accordingly, additional nonlinear control actions are designed to dominate the disturbing effect resulting from parametric uncertainty while preserving the closed-loop system stability. It will be formally proved that the robust multi-loop controller thus obtained stabilizes (globally and asymptotically) the controlled system and ensures quite interesting tracking properties. More precisely, the motor speed and (*d*-component of) stator current will both be shown to track well their references despite motor parameter uncertainties. Owing to the rectifier input current and output voltage, it will be demonstrated that the corresponding steady-state tracking errors are both harmonic signals with amplitudes depending, among others, on the supply net frequency. The larger the net frequency is, the smaller the tracking error amplitudes. Accordingly, if the net frequency is large enough the PFC requirement will actually be guaranteed up to a harmonic error of insignificant amplitude. This formally establishes the existence of the so-called ripples (usually observed in similar practical applications) and proves why this phenomenon is generally insignificant. These theoretical results are obtained making judicious use of adequate control theory tools including averaging theory and Lyapunov stability (Khalil, 2003). The paper is organized as follows: the system under study (i.e. the AC/DC/AC converter and synchronous motor association) is modeled and given a state space representation in Section 2; the controller design and the closed-loop system analysis are dealt with in Section 3; the controller performances are illustrated through numerical simulations in Section 4. For convenience, the main notations used throughout are described in Table 1.

Table 1
Main notations.

c_i, b, k_i	Design parameters
F	Combined rotor and load viscous friction
i_d, i_q	d- and q-axis stator currents
i_e	Rectifier input current
J	Combined rotor and load inertia
K	Control action generated by the DC link voltage regulator
K_M	Flux motor constant
L, R	Inductance and resistance of stator winding (PMSM)
C, L_1	Passive components of input converter
p	Number of pole pairs
$s \in (-1, +1)$	PWM input signal controlling converter IGBTs
T_L	Machine load torque
T_m	Motor torque
u_i $(i=1,2,3)$	Average values of s, u_q, u_d over cutting periods (duty ratios)
v_d, v_q	d- and q-axis stator voltages
v_{dc}	Rectifier output voltage
v_{dcref}	Reference value of rectifier output voltage v_{dc}
v_e	AC line voltage
V_i	Lyapunov functions introduced in controller design $(i=1 \ldots 5)$
x_1	Average rectifier input current, $x_1 = \bar{i}_e$
x_1^*	Input current reference, $x_1^* = k v_e$
x_2	Rectifier output voltage, $x_2 = v_{dc}$
x_3	Rotor speed, $x_3 = \omega$
x_4	q-Axis stator current, $x_4 = i_q$
x_5	d-Axis stator current, $x_5 = i_d$
y	Squared DC link voltage, $y = x_2^2 = v_{dc}^2$
y_{ref}	Reference value of y; $y_{ref} = v_{dcref}^2$
z_1	Input current tracking error, $z_1 = x_1 = x_1^*$
z_2	Squared DC link voltage error, $z_2 = y - y_{ref}$
z_3	Rotor speed tracking error, $z_3 = \omega - \omega_{ref}$
z_5	d-Axis current tracking error, $z_5 = i_d - i_{dref}$
ω	Machine rotor angular velocity
ω_e	Power supply net frequency
ε	Inverse of supply net frequency *i.e.* $\varepsilon = 1/\omega_e$

2. Modeling the 'AC/DC/AC converter-synchronous motor' association

The controlled system is illustrated by Fig. 2. It includes an AC/DC boost rectifier, on one hand, and a combination 'inverter-synchronous motor', on the other hand. The inverter is a DC/AC converter operating, like the AC/DC rectifier, according to the known pulse wide modulation (PWM) principle.

2.1. AC/DC rectifier modeling

The power supply net is connected to an H-bridge converter which consists of four IGBTs with anti-parallel diodes for bidirectional power flow mode. This is expected to accomplish two main tasks: (i) providing a constant DC link voltage and (ii) providing an almost unitary power factor. Applying Kirchhoff's laws, this subsystem is described by the following set of differential equations:

$$\frac{di_e}{dt} = \frac{v_e}{L_1} - \frac{1}{L_1} s v_{dc} \tag{1a}$$

$$\frac{dv_{dc}}{dt} = \frac{1}{2C} s i_e - \frac{1}{2C} i_s \tag{1b}$$

where i_e is the current in inductor L_1, v_{dc} denotes the voltage in capacitor $2C$, i_s designates the inverter input current, $v_e = \sqrt{2} E \cos(\omega_e t)$ is the sinusoidal net voltage (with known constants E, ω_e) and s is the switch position function taking values in the discrete set $\{-1,1\}$. Specifically:

$$s = \begin{cases} 1 & \text{if } S \text{ is ON and } S' \text{ is OFF} \\ -1 & \text{if } S \text{ is OFF and } S' \text{ is ON} \end{cases} \tag{1c}$$

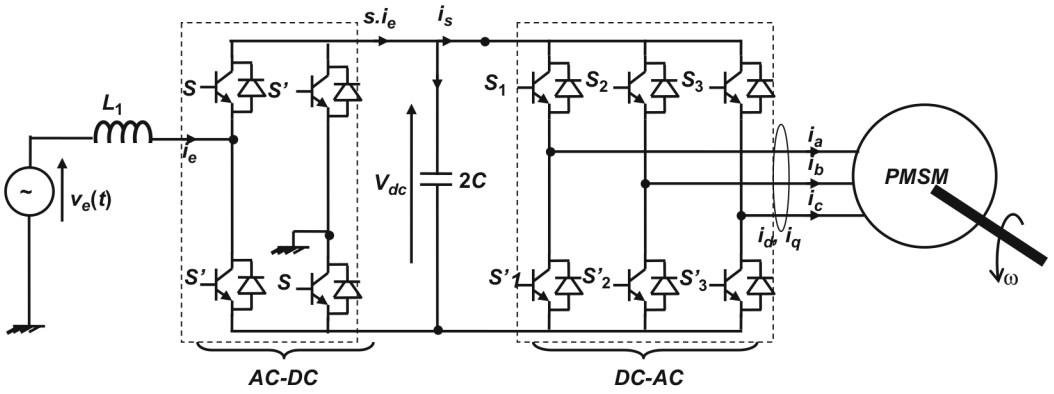

Fig.2. AC/DC/AC drive circuit with three-level inverter.

The above (instantaneous) model describes accurately the physical inverter. Then, it is based upon when constructing converter simulators. However, it is not suitable for control design due to the binary nature of the control input s. As a matter of fact, most existing nonlinear control approaches apply to systems with continuous control inputs. Therefore, control design for the above inverter will be performed using the following average version of (1a)–(1b) (Sira & Silva, 2006):

$$\frac{dx_1}{dt} = \frac{v_e}{L_1} - \frac{1}{L_1} u_1 x_2 \tag{2a}$$

$$\frac{dx_2}{dt} = \frac{1}{2C} u_1 x_1 - \frac{1}{2C} \bar{i}_s \tag{2b}$$

$$x_1 = \bar{i}_e, \quad x_2 = \bar{v}_{dc}, \quad u_1 = \bar{s} \tag{2c}$$

where x_1, x_2 and u_1 denote average values over cutting periods of i_e, v_{dc} and s, respectively.

2.2. Inverter-motor modeling

Such modeling is generally performed in the d–q rotating reference frame because the resulting components i_d and i_q turn out to be DC currents. It is shown in many places (e.g. Wallmark, 2004) that the synchronous motor model, expressed in the d–q coordinates, is given the following state space form:

$$\frac{d\omega}{dt} = -\frac{F}{J}\omega + \frac{3K_M}{2J} i_q - \frac{T_L}{J} \tag{3a}$$

$$\frac{di_q}{dt} = -\frac{R}{L} i_q - p\omega i_d - \frac{K_M}{L}\omega + \frac{1}{L} v_q \tag{3b}$$

$$\frac{di_d}{dt} = -\frac{R}{L} i_d + p\omega i_q + \frac{1}{L} v_d \tag{3c}$$

where v_d, v_q denote the averaged stator voltage in dq-coordinate (Park's transformation of the triphase stator voltages). The inverter is featured by the fact that the stator d- and q-voltage can be controlled independently. To this end, these voltages are expressed in function of the corresponding control action (see e.g. Michael, Ryan, & Rik, 1998):

$$v_q = v_{dc} u_2 \tag{4a}$$

$$v_d = v_{dc} u_3 \tag{4b}$$

$$i_s = \frac{3}{2}(u_2 i_q + u_3 i_d) \tag{4c}$$

with

$$u_2 = \bar{u}_q, \quad u_3 = \bar{u}_d \tag{4d}$$

The latter represent the average d- and q-axis (Park's transformation) of the triphase duty ratio system (s_1,s_2,s_3). The latter are defined (1c) replacing there S and S' by S_i and S'_i (i=1,2,3). Now, let us introduce the state variables:

$$x_3 = \omega, \quad x_4 = i_q, \quad x_5 = i_d \tag{4e}$$

Then, substituting (4a)–(4b) in (3a)–(3c) yields the following state space representation of the association 'inverter-motor':

$$\frac{dx_3}{dt} = -\frac{F}{J} x_3 + \frac{3K_M}{2J} x_4 - \frac{T_L}{J} \tag{5a}$$

$$\frac{dx_4}{dt} = -\frac{R}{L} x_4 - p x_3 x_5 - \frac{K_M}{L} x_3 + \frac{1}{L} u_2 x_2 \tag{5b}$$

$$\frac{dx_5}{dt} = -\frac{R}{L} x_5 + p x_3 x_4 + \frac{1}{L} u_3 x_2 \tag{5c}$$

The state space equations obtained up to now are put together to get a state-space model of the whole system including the AC/DC/AC converters combined with the synchronous motor. For convenience, the whole model is rewritten here for future reference:

$$\frac{dx_1}{dt} = \frac{v_e}{L_1} - \frac{1}{L_1} u_1 x_2 \tag{6a}$$

$$\frac{dx_2}{dt} = \frac{1}{2C} u_1 x_1 - \frac{3}{4C}(u_3 x_5 + u_2 x_4) \tag{6b}$$

$$\frac{dx_3}{dt} = -\frac{F}{J} x_3 + \frac{3K_M}{2J} x_4 - \frac{T_L}{J} \tag{6c}$$

$$\frac{dx_4}{dt} = -\frac{R}{L} x_4 - p x_3 x_5 - \frac{K_M}{L} x_3 + \frac{1}{L} u_2 x_2 \tag{6d}$$

$$\frac{dx_5}{dt} = -\frac{R}{L} x_5 + p x_3 x_4 + \frac{1}{L} u_3 x_2 \tag{6e}$$

3. Controller design

3.1. Control objectives

There are two operational control objectives:

(i) Speed regulation: the machine speed ω must track, as closely as possible, a given reference signal ω_{ref}.
(ii) PFC requirement: the rectifier input current i_e must be sinusoidal and in phase (or in opposite-phase) with the AC supply voltage v_e.

As there are three inputs at hand, namely u_1, u_2 and u_3, two additional control objectives are sought:

(iii) Controlling the continuous voltage v_{dc} making it track a given reference signal v_{dcref}. This is generally set to a constant value equal to the nominal voltage entering the inverter.
(iv) Regulating the current i_d to a reference value i_{dref}, preferably equal to zero in order to guarantee the absence of d-axis stator current. This requirement is motivated by the fact that the developed torque is given by the relation $T_m=3(K_M i_q+p(L_d-L_q)i_d i_q)/2$, see e.g. Muhammad and Rashid (2001). Accordingly, torque control should be performed acting on both i_d and i_q. But, for the surface-magnet synchronous motor, the large effective airgap means that $L_d \approx L_q = L$, i.e. i_d does not significantly influence T_m and so it is sufficient to regulate it to zero.

3.2. AC/DC rectifier control design

3.2.1. Controlling rectifier input current to meet PFC

The PFC objective means that the input current rectifier should be sinusoidal and in phase with the AC supply voltage. Accordingly, the current x_1 must be forced to tack a reference signal x_1^* of the form:

$$x_1^* = kv_e \tag{7}$$

At this point k is any positive parameter that is allowed to be time-varying. Introduce the tracking error:

$$z_1 = x_1 - x_1^* \tag{8}$$

In view of (6a), the above error undergoes the following equation:

$$\dot{z}_1 = \frac{v_e}{L_1} - \frac{1}{L_1}u_1 x_2 - \dot{x}_1^* \tag{9}$$

To get a stabilizing control law for this first-order system, consider the quadratic Lyapunov function $V_1=0.5z_1^2$. It can be easily checked that the time-derivative $\dot{V}_1$ is a negative definite function of z_1 if the control input is chosen to be

$$u_1 = \frac{L_1(c_1 z_1 + (v_e/L_1) - \dot{x}_1^*)}{x_2} \quad (c_1 > 0). \tag{10}$$

The properties of this control law are summarized in the following proposition.

Proposition 1. *Consider the system, next called current (or inner) loop, composed of the current Eq.* (6a) *and the control law* (10) *where $c_1 > 0$ is arbitrarily chosen by the user. If the reference $x_1^* = kv_e$ and its first time derivative are available then one has the following properties*:

(i) *The current loop undergoes the equation $\dot{z}_1 = -c_1 z_1$ with $z_1 = x_1 - x_1^*$. As c_1 is positive this equation is globally exponentially stable, i.e. z_1 vanishes exponentially, whatever the initial conditions.*
(ii) *If in addition k converges (to a finite value), then the PFC requirement is asymptotically fulfilled in average, i.e. the (average) input current x_1 tends (exponentially fast) to its reference kv_e as $t \to \infty$.*

3.2.2. DC link voltage regulation

The aim is now to design a tuning law for the ratio k in (7) so that the rectifier output voltage $x_2 = \overline{v}_{dc}$ is steered to a given reference value v_{dcref}. As mentioned above, v_{dcref} is generally (not mandatory) chosen to be the constant nominal inverter input voltage amplitude (i.e. the nominal stator voltage).

3.2.2.1. Relationship between k and x_2. The first step in designing such a loop is to establish the relation between the ratio k (control input) and the output voltage x_2. This is the subject of the following proposition.

Proposition 2. *Consider the power rectifier described by* (6a)–(6b) *together with the control law* (10)*. Under the same assumptions as in Proposition* 1*, one has the following properties*:

(1) *The output voltage x_2 varies, in response to the tuning ratio k, according to the equation:*

$$\frac{dx_2}{dt} = \frac{1}{2Cx_2}(kv_e^2 + z_1 v_e) - \frac{3}{4C}(u_3 x_5 + u_2 x_4) \tag{11}$$

(2) *The squared voltage ($y=x_2^2$) varies, in response to the tuning ratio k, according to the equation*:

$$\frac{dy}{dt} = \frac{1}{C}kv_e^2 + \frac{1}{C}z_1 v_e + \chi(x,t) \tag{12}$$

with

$$\chi(x,t) = -\frac{3}{2C}x_2(u_3 x_5 + u_2 x_4) \tag{13}$$

Proof. *Part 1*: The power absorbed by the AC/DC rectifier is given by the well known expression $P_{absobed}=x_1 v_e$. On the other hand, the power released by the rectifier (toward the load including the capacity and the inverter) is given by $P_{released}=u_1 x_1 x_2$. Using the power conservatism principle, one has $P_{absorbed}=P_{released}$ or, equivalently:

$$x_1 v_e = u_1 x_1 x_2 \tag{14}$$

Also, from (7) to (8) one immediately gets that $x_1=kv_e+z_1$ which together with (14) yields $u_1 x_1 = (kv_e^2 + z_1 v_e)/x_2$. This establishes (11) due to (6b).

Part 2: Deriving $y=x_2^2$ with respect to time and using (11) yields relation (12) and completes the proof of Proposition 2. □

3.2.2.2. Squared DC-link voltage regulation. The ratio k stands up as a virtual control signal in the first-order system defined by (12). As mentioned before, the reference signal $y_{ref} \overset{def}{=} v_{dcref}^2$ (of the squared DC-link voltage $x_2=v_{dc}$) is chosen to be constant (i.e. $\dot{y}_{ref}=0$), it is given the nominal inverter input voltage value. Then, it follows from (12) that the tracking error $z_2=y-y_{ref}$ undergoes the following equation:

$$\dot{z}_2 = \frac{1}{C}E^2 k + \frac{1}{C}E^2 k\cos(2\omega_e t) + \frac{\sqrt{2}E}{C}z_1\cos(\omega_e t) + \chi(x,t) - \dot{y}_{ref} \tag{15}$$

where the fact that $v_e = \sqrt{2}E\cos(\omega_e t)$ and $v_e^2 = E^2(1+\cos(2\omega_e t))$. To get a stabilizing control law for the system (15), consider the following quadratic Lyapunov function:

$$V_2 = 0.5z_2^2 \tag{16}$$

It is easily checked that the time-derivative $\dot{V}_2$ can be made negative definite in the state z_2 by letting:

$$kE^2 + kE^2\cos(2\omega_e t) + \sqrt{2}Ez_1\cos(\omega_e t) = C(-c_2 z_2 - \chi(x,t)) + C\dot{y}_{ref} \tag{17a}$$

where $c_2 > 0$ is a design parameter. The point is that such equation involves a periodic singularity due to the mutual neutralization of the first two terms on the left side of (17a). To get off this singularity and, besides, to avoid an excessive chattering in the solution, the two terms in $\cos(\cdot)$, on the left side of (17a), are just ignored. Therefore, the following approximate and simple solution is considered:

$$k = \frac{C}{E^2}(-c_2 z_2 - \chi(x,t)) + \frac{C}{E^2}\dot{y}_{ref} \tag{17b}$$

Bearing in mind the fact that the first derivative of the control ratio k must be available (Proposition 1), the following filtered version of the previous solution is adopted:

$$\dot{k}+bk=b\frac{C}{E^2}(-c_2z_2-\chi(x,t))+b\frac{C}{E^2}\dot{y}_{ref} \tag{18}$$

At this point, the regulator parameters (b,c_2) are any positive real constants. The proof of the forthcoming Theorem 1 will make it clear how these should be chosen for the control objectives to be achieved. For now, let us summarize our main findings in the following proposition.

Proposition 3. *Consider the control system consisting of the AC/DC rectifier described by* (6a)–(6b) *together with the control laws* (10) *and* (18). *Using Proposition* 1 (*Part* 1), *it follows that the closed-loop undergoes, in the* (z_1,z_2,k)*-coordinates, the following equation where* $z_1=x_1-x_1^*$ *and* $z_2=y-y_{ref}$:

$$\begin{pmatrix}\dot{z}_1\\ \dot{z}_2\\ \dot{k}\end{pmatrix}=\begin{pmatrix}-c_1 & 0 & 0\\ 0 & 0 & \frac{E^2}{C}\\ 0 & -\frac{bC}{E^2}c_2 & -b\end{pmatrix}\begin{pmatrix}z_1\\ z_2\\ k\end{pmatrix}+\begin{pmatrix}0\\ 1\\ -\frac{bC}{E^2}\end{pmatrix}\chi(x,t)+\begin{pmatrix}0\\ \frac{E^2}{C}k\cos(2\omega_e t)+\frac{\sqrt{2}}{C}Ez_1\cos(\omega_e t)0\end{pmatrix}-\begin{pmatrix}0\\ 1\\ -\frac{bC}{E^2}\end{pmatrix}\dot{y}_{ref} \tag{19}$$

The stability of the error system defined by (19) will be fully analyzed later. But, first, the controller development must be completed.

3.3. Robust control design of the 'inverter-motor' set

3.3.1. Motor model with parameter uncertainties

The mechanical motor parameters T_L (load torque) and F (viscous friction coefficient), are not supposed to be accurately known. These are just supposed to be varying within known intervals. Specifically, it is assumed that

$$F=F_0(1+\Delta_F) \tag{20a}$$

$$T_L=T_{L0}(1+\Delta_T) \tag{20b}$$

where (F_0,T_{L0}) denote nominal values and (Δ_F,Δ_T) are possibly varying uncertainties such that

$$\Delta_F^{\mathrm{MIN}}\le\Delta_F\le\Delta_F^{\mathrm{MAX}};\quad \Delta_T^{\mathrm{MIN}}\le\Delta_T\le\Delta_T^{\mathrm{MAX}} \tag{21}$$

where Δ^{MIN} and Δ^{MAX} are known bounds. Using (20), Eq. (6c) can be rewritten as follows:

$$\frac{dx_3}{dt}=-\frac{F_0}{J}x_3+\frac{3K_M}{2J}x_4-\frac{T_{L0}}{J}+\Delta_1x_3+\Delta_2 \tag{22}$$

with

$$\begin{cases}\Delta_1=-\frac{F_0}{J}\Delta_F\\ \Delta_2=-\frac{T_{L0}}{J_0}\Delta_L\end{cases} \tag{23}$$

Substituting (22) in (6c)–(6e) gives a new model representation of the motor:

$$\frac{dx_3}{dt}=-\frac{F_0}{J}x_3+\frac{3K_M}{2J}x_4-\frac{T_{L0}}{J}+\varphi_1^T\Delta \tag{24a}$$

$$\frac{dx_4}{dt}=-\frac{R}{L}x_4-px_3x_5-\frac{K_M}{L}x_3+\frac{1}{L}u_2x_2 \tag{24b}$$

$$\frac{dx_5}{dt}=-\frac{R}{L}x_5+px_3x_4+\frac{1}{L}u_3x_2 \tag{24c}$$

with

$$\varphi_1=\begin{bmatrix}x_3 & 1\end{bmatrix}^T,\quad \Delta=\begin{bmatrix}\Delta_1 & \Delta_2\end{bmatrix}^T \tag{25}$$

3.3.2. Robust motor speed control

Based on Eqs. (24a)–(24b), a control law will now be determined, for the control input u_2, in order to guarantee a satisfying speed reference tracking quality, despite the motor parameter uncertainties. Following the robustified backstepping design technique (Krstic et al., 1995), let us introduce the speed tracking error:

$$z_3=x_3-\omega_{ref} \tag{26}$$

In view of (24a), the above error undergoes the following equation:

$$\dot{z}_3=-\frac{F_0}{J}x_3+\frac{3K_M}{2J}x_4-\frac{T_{L0}}{J}-\dot{\omega}_{ref}+\varphi_1^T\Delta \tag{27}$$

In (27), the quantity $\alpha=(3K_M/(2J))x_4$ stands up as a (virtual) control input for the z_3-dynamics. Let α^* denote the associated stabilizing function. Eq. (27) suggests the following choice:

$$\alpha^*=-c_3z_3-k_1|\varphi_1|^2z_3+\frac{F_0}{J}x_3+\frac{T_{L0}}{J}+\dot{\omega}_{ref} \tag{28}$$

where $|\varphi_1|$ denotes the Euclidean norm of φ_1, $c_3>0$ is a design parameter and $k_1|\varphi_1|^2z_3$ a nonlinear damping term introduced to dominate the uncertain term $\varphi_1^T\Delta$. If α were let equal to α^*, one would have

$$\dot{z}_3=-c_3z_3-(k_1|\varphi_1|^2z_3-\varphi_1^T\Delta) \tag{29}$$

Then, considering the Lyapunov function candidate:

$$V_3=0.5z_3^2 \tag{30}$$

One would get the following time-derivative along the trajectory of (27):

$$\dot{V}_3=z_3\dot{z}_3=-c_3z_3^2-(k_1|\varphi_1|^2z_3-\varphi_1^T\Delta)z_3 \tag{31}$$

which shows that $\dot{V}_3$ is a negative definite function of z_3 in case $\Delta=0$. As $\alpha=(3K_M/(2J))x_4$ is a virtual control input, one cannot set $\alpha=\alpha^*$. Nevertheless, the above expression of the desired trajectory is retained and a new error is introduced, i.e.

$$z_4=\alpha-\alpha^* \tag{32}$$

Using (28)–(32), it follows from (27) that the z_3-dynamics undergoes the following equation:

$$\dot{z}_3=-c_3z_3-(k_1|\varphi_1|^2z_3-\varphi_1^T\Delta)+z_4 \tag{33}$$

The next step consists in determining the control input u_2 so that the errors (z_3,z_4) vanish asymptotically. The trajectory of the error z_4 is first obtained by time-deriving (32):

$$\dot{z}_4=(3K_M/(2J))\dot{x}_4-\dot{\alpha}^* \tag{34}$$

Using (28) and (24a)–(24b) in (34) yields

$$\dot{z}_4=\beta(x)-\ddot{\omega}_{ref}-(c_3+k_1|\varphi_1|^2)^2z_3+(c_3+k_1|\varphi_1|^2)z_4+\varphi_2^T\Delta+\gamma u_2 \tag{35}$$

with

$$\beta(x) = -\frac{3K_M}{2J}\left(\frac{R}{L}x_4 + px_3x_5 + \frac{K_M}{L}x_3\right) + \left(2k_1x_3z_3 - \frac{F_0}{J}\right)\left(-\frac{F_0}{J}x_3 + \frac{3K_M}{2J}x_4 - \frac{T_{L0}}{J}\right) \tag{36}$$

$$\varphi_2 = \left(c_3 + k_1|\varphi_1|^2 + 2k_1x_3z_3 - \frac{F_0}{J}\right)\varphi_1, \quad \gamma = \frac{3K_M}{2J}\frac{x_2}{L} \tag{37}$$

For convenience, the error equations (33) and (35) are rewritten together as

$$\dot{z}_3 = -(c_3 + k_1|\varphi_1|^2)z_3 - \varphi_1^T\Delta + z_4 \tag{38a}$$

$$\dot{z}_4 = \beta(x) - \ddot{\omega}_{ref} - (c_3 + k_1|\varphi_1|^2)^2 z_3 + (c_3 + k_1|\varphi_1|^2)z_4 + \varphi_2^T\Delta + \gamma u_2 \tag{38b}$$

To determine a stabilizing control law for (38a)–(38b), let us consider the following Lyapunov function candidate:

$$V_4 = V_3 + 0.5z_4^2 \tag{39}$$

Using (33), the time-derivative of V_4 turns out to be

$$\dot{V}_4 = -(c_3 + k_1|\varphi_1|^2)z_3^2 + \varphi_1^T\Delta z_3 + z_3z_4 + z_4\dot{z}_4 \tag{40}$$

Combining (38b) and (40) yields

$$\dot{V}_4 = -(c_3 + k_1|\varphi_1|^2)z_3^2 + (\varphi_1^Tz_3 + \varphi_2^Tz_4)\Delta + [z_3 + \beta(x) + \ddot{\omega}_{ref} - (c_3 + k_1|\varphi_1|^2)^2 z_3 + (c_3 + k_1|\varphi_1|^2)z_4 + \gamma u_2]z_4 \tag{41}$$

This shows that for the (z_3,z_4)-system to be asymptotically stable, it is sufficient to choose the control u_2 as follows:

$$u_2 = \gamma^{-1}[-z_3 - \beta(x) + \ddot{\omega}_{ref} + (c_3 + k_1|\varphi_1|^2)^2 z_3 - (c_3 + k_1|\varphi_1|^2)z_4 - (c_4 + k_2|\varphi_2|^2)z_4] \tag{42}$$

where $c_4 > 0$ is a new design parameter and $k_2|\varphi_2|^2z_4$ an additional nonlinear damping term introduced to dominate the uncertain term $\varphi_2\Delta$ in Eq. (35). From (41) and (42) one gets

$$\dot{V}_4 = -c_3z_3^2 - c_4z_4^2 - k_1|\varphi_1|^2z_3^2 - k_2|\varphi_2|^2z_4^2 + (\varphi_1^Tz_3 + \varphi_2^Tz_4)\Delta \tag{43}$$

The stability analysis of the closed-loop system consisting of the subsystem (24a)–(24b) and the regulator (42) will be performed later (see Theorem 1). But first let us end up the controller development by designing a control law for the remaining input, i.e. u_3.

3.3.2. d-Axis current regulation

The d-axis current x_5 undergoes Eq. (24c) in which the following quantity:

$$v = \frac{1}{L}(px_3x_4 + u_3x_2) \tag{44a}$$

acts as a virtual input. As the reference signal i_{dref} is null, it follows that the tracking error $z_5 = x_5 - i_{dref}$ undergoes the equation:

$$\dot{z}_5 = -\frac{R}{L}z_5 + v \tag{44b}$$

To get a stabilizing control signal for this first-order system, consider the following quadratic Lyapunov function:

$$V_5 = 0.5z_5^2 \tag{45}$$

It can be easily checked that the time-derivative $\dot{V}_5$ can be made equal to $-c_5z_5^2$ letting the (virtual) control input be generated by the following control law:

$$v = \frac{R}{L}z_5 - c_5z_5 \quad (\text{with } c_5 > 0 \text{ a design parameter}) \tag{46}$$

Now, it is readily observed that the actual control input is obtained substituting (46) in (44) and solving the resulting equation with respect in u_3. Doing so, one gets:

$$u_3 = \frac{L}{x_2}\left(-c_5z_5 + \frac{R}{L}x_5 - px_3x_4\right) \tag{47}$$

Finally, combining (46) and (44b) gives

$$\dot{z}_5 = -c_5z_5 \tag{48}$$

The speed and d-axis current control laws, defined by (42) and (47) are now analyzed in the following theorem.

Theorem 1. *Consider the control system consisting of the subsystem* (24a)–(24c) *and the control laws* (42) *and* (47).

(1) *The resulting closed-loop system undergoes, in the* (z_3,z_4,z_5)*-coordinates, the following equation:*

$$\dot{z}_3 = -(c_3 + k_1|\varphi_1|^2)z_3 - \varphi_1^T\Delta + z_4 \tag{49a}$$

$$\dot{z}_4 = -(c_4 + k_2|\varphi_2|^2)z_4 - \varphi_2^T\Delta \tag{49b}$$

$$\dot{z}_5 = -c_5z_5 \tag{49c}$$

with $z_3 = x_3 - \omega_{\mathrm{ref}}$, $z_4 = (3K_M/(2J))x_4 - \alpha^*$, $z_5 = x_5 - i_{dref}$, $\alpha^* = -c_3z_3 - k_1|\varphi_1|^2z_3 + (F_0/J)x_3 + (T_{L0}/J) + \dot{\omega}_{ref}$.

(2) *The error vector* (z_3,z_4,z_5) *converges exponentially to a compact neighborhood of the origin* [0 0 0] *and the size of this compact can be made arbitrarily small by choosing the design parameters* (k_1,k_2) *and* (c_3,c_4,c_5) *sufficiently large.*

(3) *In the case of no motor parameter uncertainties, i.e.* $\Delta = [0 \quad 0]^T$, *the origin* [0 0 0] *is an exponentially stable equilibrium of the system* (49a)–(49c). *Consequently, the error vector* $[z_3z_4z_5]$ *vanishes exponentially fast, whatever the initial conditions.*

Proof. See Appendix A. □

3.4. PFC achievement

In the following theorem, it is shown that, for a specific class of reference signals, including periodic signals, the PFC requirement is achieved (in the mean) with an accuracy that depends, among others, on the network frequency ω_e. The following notations are needed to formulate the results:

$$Z_1 = [z_1 \quad z_2 \quad k]^T, \quad Z_2 = [z_3 \quad z_4 \quad z_5]^T \tag{50a}$$

$$a_0 = \frac{E^2}{C}, \quad a_1 = \frac{bC}{E^2}c_2, \quad a_2 = \sqrt{2}\frac{E}{C}, \quad a_3 = \frac{3}{2}\frac{b}{E^2}, \quad \varepsilon = \frac{1}{\omega_e} \tag{50b}$$

$$A = \begin{pmatrix} A_1 & O \\ O & A_2 \end{pmatrix} \in IR^{6\times 6} \text{ with } A_1 = \begin{pmatrix} -c_1 & 0 & 0 \\ 0 & 0 & a_0 \\ 0 & -a_1 & -b \end{pmatrix}, \quad A_2 = \begin{pmatrix} -c_3 & 1 & 0 \\ 0 & -c_4 & 0 \\ 0 & 0 & -c_5 \end{pmatrix} \tag{50c}$$

$$f(Z,t) = \begin{bmatrix} 0 & (a_0k\cos(2\omega_et) + a_2z_1\cos(\omega_et)) & 0 & 0 & 0 & 0 \end{bmatrix}^T \in IR^6 \tag{50d}$$

$$g = \begin{bmatrix} 0 & \frac{-3}{2C} & a_3 & 0 & 0 & 0 \end{bmatrix}^T \in IR^6 \tag{50e}$$

$$h = \begin{bmatrix} 0 & 1 & -\frac{bC}{E^2} & 0 & 0 & 0 \end{bmatrix}^T \in IR^6 \tag{50f}$$

$$\sigma(Z_2,t)=(R-Lc_5)z_5^2+\frac{4J^2L}{9K_M^2}\left\{z_4+\left(\frac{F}{J}-c_3\right)z_3+\frac{F}{J}\omega_{ref}+\frac{T_L}{J}+\dot{\omega}_{ref}\right\}$$
$$\times\left\{-\left(c_3+c_4-\frac{R}{L}-\frac{F}{J}\right)z_4+\left(c_3^2-1-c_3\left(\frac{R}{L}+\frac{F}{J}\right)+\frac{RF}{JL}+\frac{3K_M^2}{2JL}\right)z_3\right.$$
$$\left.+\frac{RT_L}{LJ}+\left(\frac{RF}{JL}+\frac{3K_M^2}{2JL}\right)\omega_{ref}+\frac{\dot{T}_L}{J}+\left(\frac{R}{L}+\frac{F}{J}\right)\dot{\omega}_{ref}+\ddot{\omega}_{ref}\right\} \quad (50g)$$

$$\varphi=[0\quad 0\quad 0\quad -k_1|\varphi_1|^2\quad -k_2|\varphi_2|^2\quad 0]^T\in IR^6 \quad (50h)$$

$$\Phi=[0_3\quad 0_3\quad 0_3\quad \varphi_1\quad \varphi_2\quad 0_3]^T\in IR^{6\times 3}\ \text{with}\ 0_3=[0\quad 0\quad 0]^T \quad (50i)$$

Theorem 2. *Consider the system including the AC/DC/AC power converters and the synchronous motor, connected in tandem as shown in Fig. 2. For control design purpose, the system is represented by its average model* (6a)–(6e). *Let the reference signals* v_{dcref}, ω_{ref} *and* i_{dref} *be selected such that* $v_{dcref}>0$,$\omega_{ref}\geq 0$ *and* $i_{dref}=0$. *Consider the controller defined by the control laws* (10), (42) *and* (47) *where all design parameters* (*i.e.* c_1,c_2,c_3,c_4,c_5,k_1,k_2 *and* b) *are positive. Then, one has the following properties*:

(1) *The resulting closed-loop system undergoes the state-space equation:*

$$\dot{Z}=AZ+\varphi^TZ+\Phi\Delta+f(Z,t)+g\sigma(Z_2,t)+h\dot{y}_{ref} \quad (51)$$

(2) *Case of no motor parameter uncertainties, i.e.* $\Delta=0$. *If* v_{dcref} *and* ω_{ref}, *as well as their time-derivatives* (*up to the second order for* ω_{ref}), *are bounded and periodic signals with period* $N\pi/\omega_e$ (*for some integer N) then, there exists a positive real* ε^* *such that one has for* $0<\varepsilon<\varepsilon^*$:
   (a) *The tracking error* $z_2=y-y_{ref}$ *and the tuning parameter k are harmonic signals that continuously depend on* ε.
   (b) *Furthermore, one has*

$$\lim_{\varepsilon\to 0}z_2(t,\varepsilon)=0\quad\text{and}\quad\lim_{\varepsilon\to 0}k(t,\varepsilon)=\frac{3}{2C}\frac{\overline{\sigma}(0_3)}{a_0} \quad (52)$$

   where $\overline{\sigma}(0_3)$ denotes the mean value of the periodic time function $\sigma(0_3,t)$.

(3) *Case of constant parameter uncertainties, i.e.* Δ *not necessarily null but time-invariant. Under the same assumptions on* v_{dcref} *and* ω_{ref}, *the results of Part 2 still hold with an error that can be made arbitrarily small by letting the design parameters* (k_1,k_2) *and* (c_3,c_4,c_5) *be sufficiently large.*

Proof. See Appendix B. □

Remarks 1. (a) As a result of Theorem 1 (Parts 2 and 3), the motor speed and the d-component of its stator current both converge to their respective references (if $\Delta=0$) or sufficiently close to these references (when $\Delta\neq 0$). This is a consequence of the exponential convergence of the errors (z_3,z_5) to zero (if $\Delta=0$) or to a compact of zero the size of which can be made arbitrarily small letting the design parameters $\kappa=\min(k_1,k_2)$ and $c=\min(c_3,c_4,c_5)$ sufficiently large.

(b) From Proposition 3 one gets that the error $z_1=x_1-x_1^*=i_e-kv_e$ undergoes the equation $\dot{z}_1=-c_1z_1$ which implies that z_1 converges exponentially fast to zero. The importance of Theorem 2 (Parts 2 and 3) lies (partly) in the fact that the (time-varying) ratio k does converge to a fixed value (up to a harmonic error). This demonstrates that the PFC requirement is actually fulfilled with an accuracy that depends on ω_e. The larger ω_e is, the more accurate the PFC quality. It will be seen in the forthcoming simulation that the usual value ω_e=50 Hz leads to a quite acceptable PFC quality.

(c) Theorem 2 (Parts 2 and 3) also demonstrates that the tracking objective is achieved (in the mean) for the DC-link squared voltage $y=x_2^2=v_{dc}^2$ with an accuracy that depends on the voltage network frequency ω_e. The class of admissible references (v_{dcref}, ω_{ref}) includes periodic signals with period $N\pi/\omega_e$. That is, these signals must vary slower than the network voltage.

(d) The fact that the tracking error $z_2=v_{dc}^2-v_{dcref}^2$ is harmonic proves the existence of output ripples. Theorem 2 (Part 2) ensures that the effect of ripples is insignificant if ω_e is sufficiently large. It will be observed through simulations that the value ω_e=50 Hz leads to sufficiently small ripples.

(e) As pointed out by (20a)–(20c), parameter uncertainty in model (6a)–(6e) only concerns the mechanical parameters. The robustness of the controller (defined by (10), (42) and (47)) has been achieved resorting to the additional nonlinear damping terms (namely $k_1|\varphi_1|^2z_3$ and $k_2|\varphi_2|^2z_4$). These have been designed to dominate the parameter uncertainty effect while preserving the closed-loop system stability. As a matter of fact, the same approach could be applied mutatis-mutandis to dominate the effect of eventual electrical parameters uncertainty. This option has been discarded to keep the controller complexity at a reasonable level.

4. Simulation

The experimental setup described by Fig. 3 has been simulated, within the Matlab/Simulink environment. The system is given the following characteristics:

Supply network voltage: $v_e(t)=\sqrt{2}.E\cos(\omega_e t)$ single phase 220 V/50 Hz. AC/DC/AC converters: L_1=15 mH; C=1.5 mF; modulation frequency 10 kHz. Synchronous motor: a nominal power of 3 kW and L=9.4 mH, R=0.6 Ω, K_M=1.29, J_0=0.00765 N m/rd/s^2, F_0=0.003819 N m/rd/s, p=2.

The following values of the controller design parameters proved to be suitable: c_1=1000, c_2=40, c_3=30, c_4=900, c_5=800, b=100, k_1=10, k_2=100.

4.1. Controller tracking capability: case of no parameter uncertainties

The controller performances are evaluated in presence of time-varying rotor speed reference ω_{ref} and load torque T_L (Fig. 4). Specifically, ω_{ref} is a filtered step-like signal that steps from 0 to 100 rad/s, at t=0.2 s, and from 100 to −100 rad/s at t=1 s. The machine load torque T_L is also a filtered step-like signal that steps, at t=0.5 s, from 0 to its nominal value T_{L0}=20 N m. The involved filters are second order for ω_{ref} and first order for T_L.

The controller performances are illustrated by the curves in Fig. 5. Curves 1 and 2 show, respectively, the resulting input current i_e and the variation of the ratio k. It is seen that the current amplitude changes whenever the speed reference or the load torque vary (compare with Fig. 4). But, the current frequency is insensitive to these changes (Fig. 5(c)). Furthermore, the current remains (almost) all time in phase or opposite phase with the supply net voltage $v_e(t)$ complying with the PFC requirement. This is particularly demonstrated by Fig. 5(b) which shows that the ratio k takes a constant value, after the transient periods following changes in rotor speed reference or in load torque. This confirms Theorem 2 (Part 1) and Remark 2c. Notice that the ratio k becomes negative starting from time t=1 s because the speed reference has suddenly fallen down from 100 to −100 rad/s. Then the input

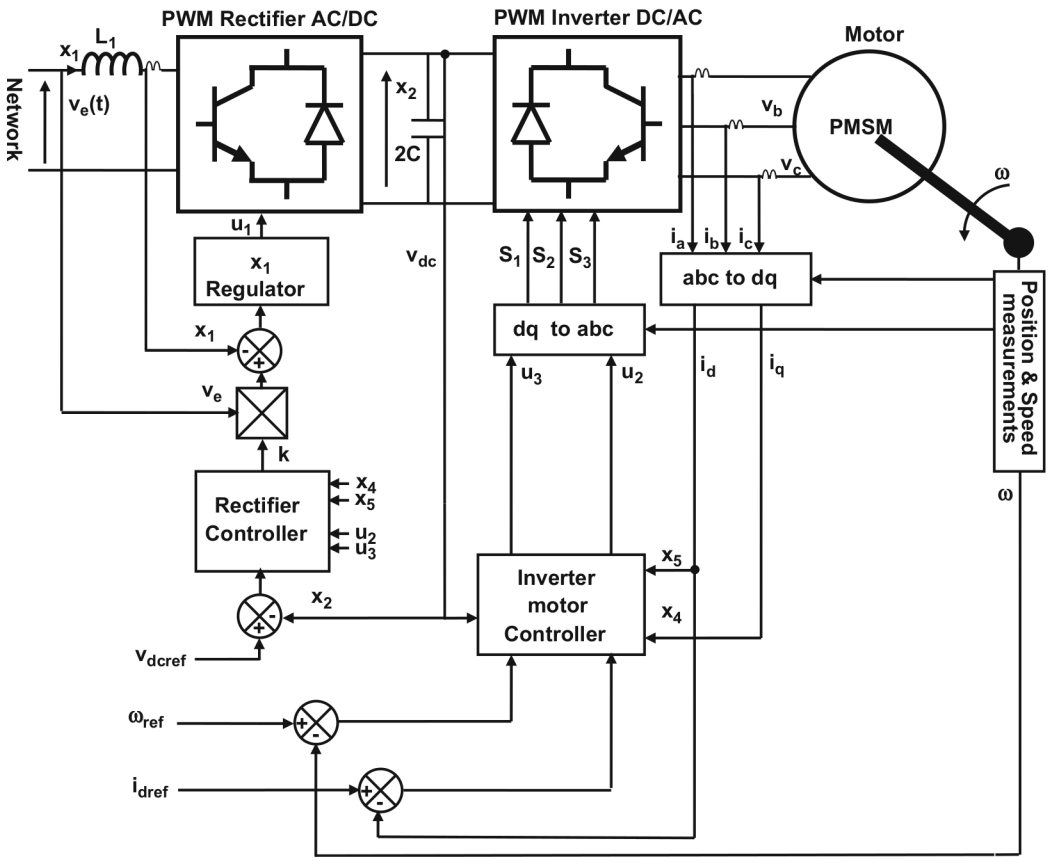

Fig. 3. Control system including AC/DC/AC converters and a synchronous motor.

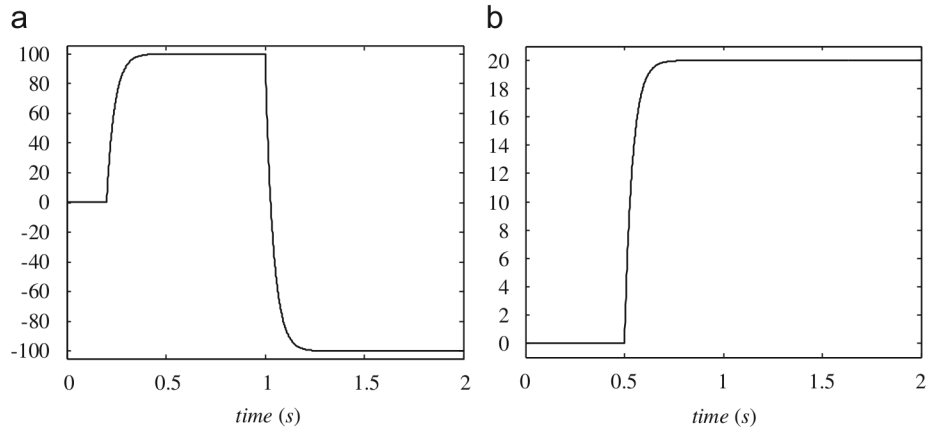

Fig. 4. (a) Rotor speed reference ω_{ref} (rd/s); (b) machine load torque T_L (Nm).

current i_e becomes in opposite phase with the supply net voltage v_e which means that the power flow sense is reversed, i.e. the power produced by the machine is transferred to the grid through the triphase inverter (which then operates as rectifier) and the single phase rectifier (which then operates as inverter).

Fig. 5(d) shows that the DC-link voltage $x_2=v_{dc}$ is tightly regulated: it quickly settles down after each change in the speed reference or load torque. As expected by Theorem 2 (Part 1), and commented in Remark 2c, the DC link voltage v_{dc} is subject to small amplitude ripples oscillating at the supply net frequency ω_e.

Figs. 5(e) and (f) show that the machine speed, $x_3=\omega$, and the d-component of the stator current, $x_5=i_d$, both perfectly converge to their respective references. These variables are subject to no ripples, confirming Theorem 1 (Part 1) and Remark 2a. The tracking quality is quite satisfactory as, for both variables, the response time (after each change in the speed reference or load torque) is less than 0.2 s.

Finally, the resulting control actions (u_1,u_2,u_3) are illustrated by Figs. 5(h)–(j). It is particularly seen from Fig. 5(h) that u_1 is (in average) sinusoidal with frequency $50\times 2\pi$(rd/s), i.e. the same frequency as the net voltage v_e. This confirms Eq. (10) considering the fact that z_1 and k both converge (respectively to zero and some constant). The control signal u_1 is (just as z_1 and k) disturbed by additive ripples. Similar comments can be made upon u_2 and u_3.

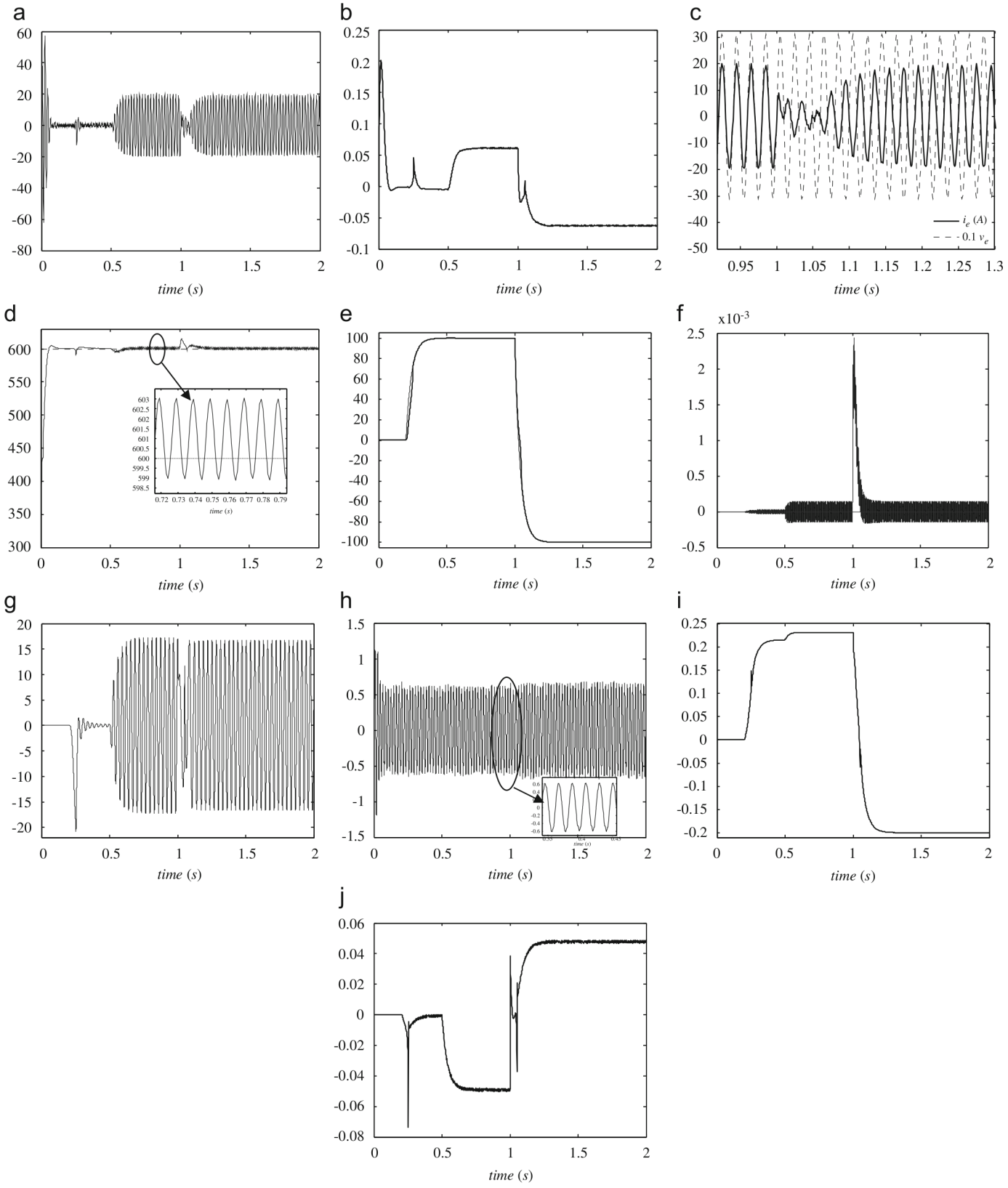

Fig.5. Tracking performances of the controller defined by (10), (42) and (47) in response to the varying speed reference and load torque of Fig. 4. Case of no parameter uncertainties. (a) Input current x_1 (A), (b) tuning parameter k, (c) unitary power factor checking (PFC), (d) DC-link voltage v_{dc} (V) and its reference (dashed), (e) rotor speed (rd/s) and its reference (dashed), (f) d-axis stator current (A) and its reference (dashed), (g) stator current i_a (A), (h) control signal u_1, (i) control signal u_2, (j) control signal u_3.

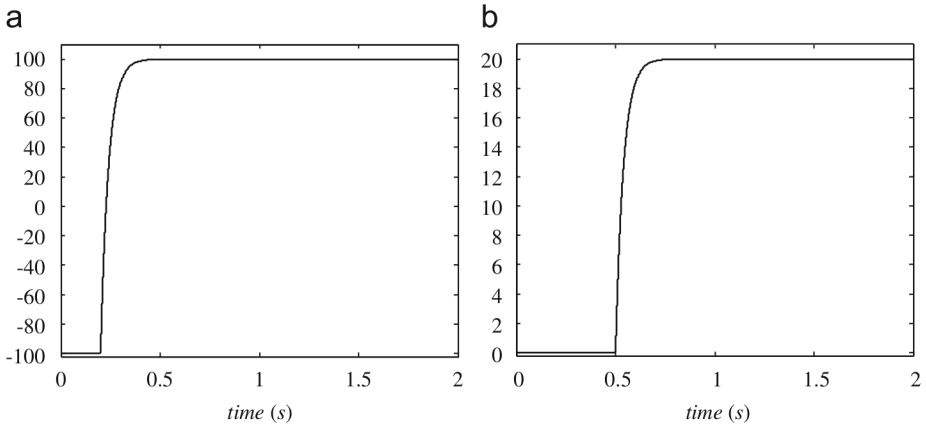

Fig. 6. Mechanical input signals: (a) rotor speed reference ω_{ref} (rd/s); (b) machine load torque T_L (N m).

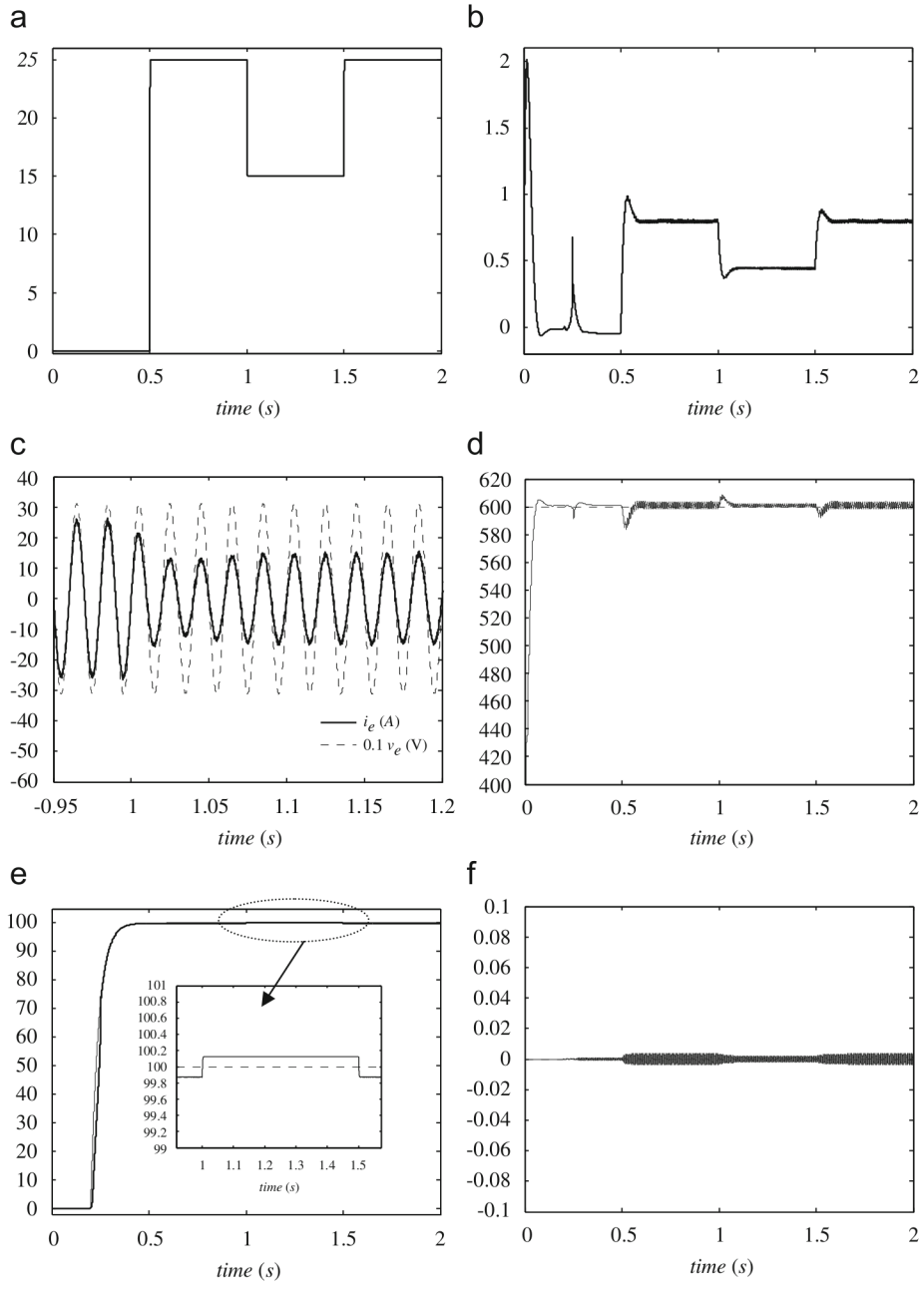

Fig. 7. Robustness of the controller defined by (10), (42) and (47) against uncertainties of 25% on the load torque changes. (a) Motor load torque (N m), (b) tuning parameter k, (c) unitary power factor checking (PFC), (d) DC-link voltage v_{dc} (V), (e) rotor speed ω (rd/s), (f) d-axis stator current (A).

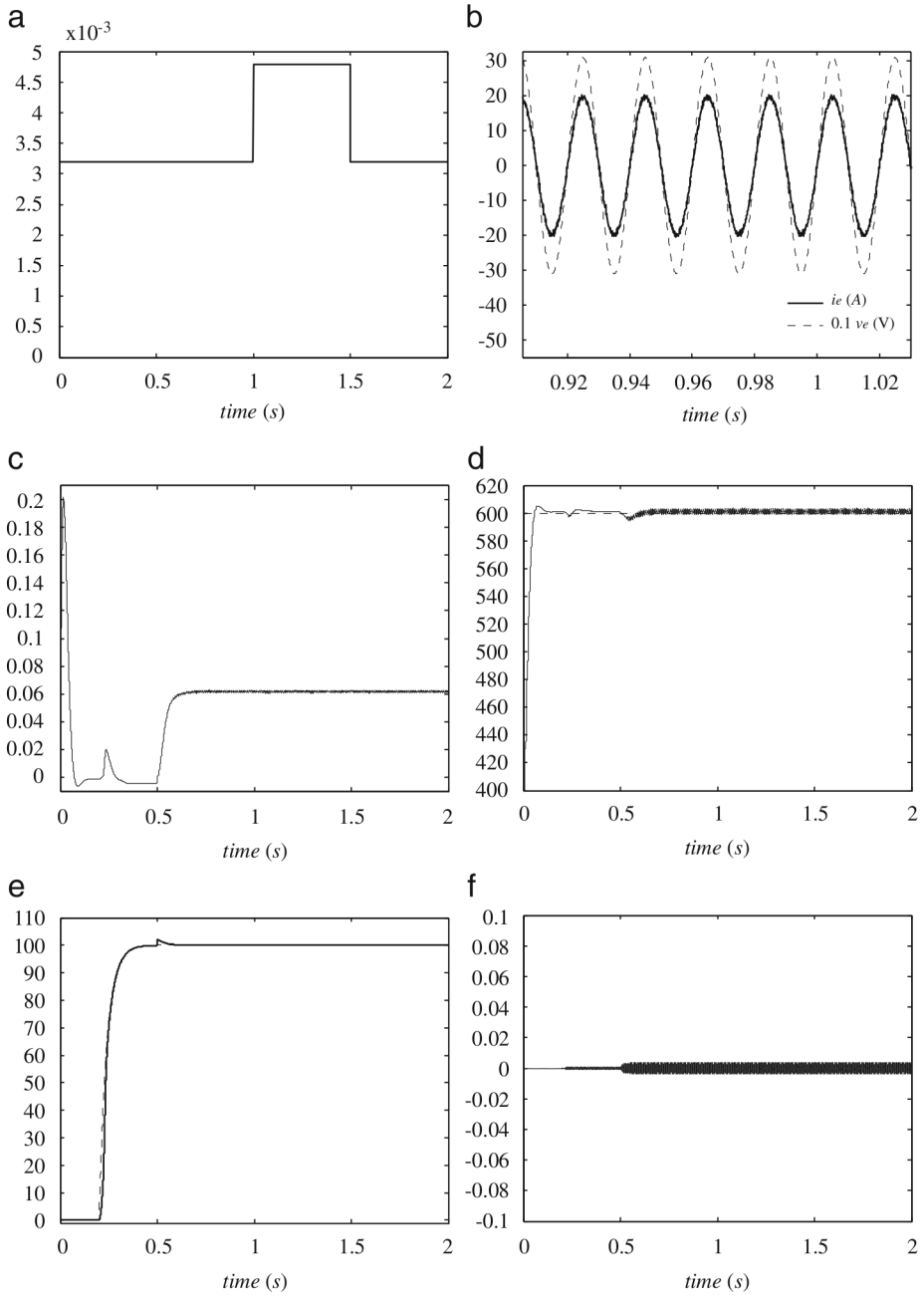

Fig. 8. Robustness of the controller defined by (10), (42) and (47) against uncertainties on viscous friction. (a) Motor friction F (N m s/rad), (b) unitary power factor checking (PFC), (c) tuning parameter k, (d) DC-link voltage v_{dc} (V), (e) rotor speed ω (rd/s), (f) d-axis stator current (A).

4.2. Controller robustness against system parameter uncertainties

The controller robustness against uncertainties on system parameters is progressively checked in the present subsection. In all forthcoming experiments, the rotor speed reference ω_{ref} and the machine load torque T_L are filtered step-like signals (Fig. 6). Specifically, ω_{ref} steps from 0 to 100 rad/s, at t=0.2 s, and T_L steps, at t=0.5 s, from 0 to its nominal value T_{L0}=20 N m. The involved filters are a second order for ω_{ref} and a first order for T_L.

Controller robustness against load torque uncertainty: The simulation protocol is such that the true load torque T_L is time-varying as shown by Fig. 7(a). But, in the controller, the load torque is still supposed to vary according to Fig. 6. A difference of 25% is observed, starting from time t=0.5 s between the supposed torque and its true value. Figs. 7(b)–(f) show that the controller ideal performances, obtained in the uncertainty-free case (Section 4.1), are well preserved in presence of load uncertainty.

Controller robustness against viscous friction coefficient: The simulation protocol is such that the true viscous friction coefficient F is changing as shown by Fig. 8(a). Accordingly, the viscous friction coefficient is subject to a variation of 50% with respect to its nominal value, 0.003819 N m/rd/s, between t=1 and 1.5 s. Such variation is entirely ignored in the controller where the nominal value is used all time. Figs. 8(b)–(f) show that the controller still performs well, despite the present uncertainty.

5. Conclusion

The problem of controlling associations including an AC/DC rectifier, a DC/AC inverter and a synchronous motor has been

addressed. The system dynamics have been described by the averaged fifth order nonlinear state-space model (6a)–(6e). The load torque and viscous friction are subject to uncertainties (20a)–(20c). Based on such a model, the multiloops nonlinear controller defined by the control laws (10), (42) and (47) has been designed by a robustified version of the backstepping design technique and analyzed using tools from the Lyapunov stability and averaging theory. It has been formally established that the proposed robust controller achieves the objectives it has been designed to: (i) almost unitary power factor; (ii) well regulated DC-link voltage (v_{dc}); (iii) satisfactory rotor speed reference tracking over a wide range of load torque variation; (iv) tight regulation of the stator d-axis current. To the author's knowledge, it is the first time that a so complete formal design and analysis framework is developed for synchronous motors control design. These results have been checked by a simulation study.

Appendix A. Proof of Theorem 1

Part 1 is immediately obtained from (33), (38) and (48). To prove Part 2, consider the Lyapunov function candidate $V=V_4+V_5=0.5(z_3^2+z_4^2+z_5^2)$. It readily follows that

$$\dot V = z_3\dot z_3 + z_4\dot z_4 + z_5\dot z_5 = -c_3z_3^2 - c_4z_4^2 - c_5z_5^2 - k_1|\varphi_1|^2z_3^2 - k_2|\varphi_2|^2z_4^2 - (\varphi_1^T z_3 + \varphi_2^T z_4)\Delta \tag{A.1}$$

$\dot V$ can be bounded from above as follows:

$$\dot V \le -c_3z_3^2 - c_4z_4^2 - c_5z_5^2 - (k_1|\varphi_1|^2z_3^2 - |\varphi_1||z_3|\|\Delta\|_\infty) - (k_2|\varphi_2|^2z_4^2 - |\varphi_2||z_4|\|\Delta\|_\infty) \tag{A.2}$$

which in turn implies:

$$\dot V \le -c_3z_3^2 - c_4z_4^2 - c_5z_5^2 - k_1\left(|\varphi_1||z_3| - \frac{\|\Delta\|_\infty}{2k_1}\right)^2 - k_2\left(|\varphi_2||z_4| - \frac{\|\Delta\|_\infty}{2k_2}\right)^2 + \frac{\|\Delta\|_\infty^2}{4k_1} + \frac{\|\Delta\|_\infty^2}{4k_2} \tag{A.3}$$

or, equivalently:

$$\dot V \le -cV + \frac{\|\Delta\|_\infty^2}{2\kappa} \tag{A.4}$$

where $\|.\|_\infty$ denotes the L_∞ norm and $c=\min(c_3,c_4,c_5)$ and $\kappa=\min(k_1,k_2)$.

Recalling that $V=0.5\sum_{i=3}^5 z_i^2$, it readily follows from (A.4) that, whatever the initial condition $(z_3(0),z_4(0),z_5(0))$ and the parameter uncertainty vector Δ, the vector $[z_3(t)z_4(t)z_5(t)]$ converges exponentially to the following compact:

$$\sum_{i=3}^5 z_i^2 \le 2\frac{\|\Delta\|_\infty^2}{c\kappa} \tag{A.5}$$

It is clear that the size of such compact is inversely proportional to $c\kappa$. This proves Part 2.

Finally, if $\Delta=0$ one gets from (A.4) that $\dot V \le -cV$ which implies that $V=0.5\sum_{i=3}^5 z_i^2$ vanishes exponentially fast. This establishes Part 3 and completes the proof of Theorem 1.

Appendix B. Proof of Theorem 2

Part 1: Substituting the right sides of (42) and (47) to u_2 and u_3 in (13), one gets:

$$\chi(x,t) = -\frac{3\sigma(Z_2,t)}{2C} \tag{B.1}$$

where we have used (50f)–(50g). Substituting the right side of (B.1) to $\chi(x,t)$ in (19) gives

$$\dot Z_1 = A_1Z_1 + \sigma(Z_2,t)\begin{bmatrix}0 & -\frac{3}{2C} & \frac{3b}{2E^2}\end{bmatrix}^T + \begin{bmatrix}0 & \frac{E^2}{C}k\cos(2\omega_e t) + \frac{\sqrt{2}}{C}Ez_1\cos(\omega_e t) & 0\end{bmatrix}^T + \begin{bmatrix}0 & -1 & \frac{bC}{E^2}\end{bmatrix}^T\dot y_{ref} \tag{B.2}$$

where notations (50b)–(50f) have been used. Putting together (B.2) and (49a)–(49c) in a global state space equation one gets (51) and proves Part 1.

Part 2: As v_{dcref}, ω_{ref} and T_L as well as their derivatives are constant or periodic (with period $N\pi/\omega_e$), it follows that the system (51) is periodically time-varying. Therefore, the averaging theory turns out to be a suitable framework to analyze its stability (see e.g. Khalil, 2003). To this end, introduce the time-scale change $\tau=\omega_e t$ and the following signal changes:

$$W(\tau)=Z(t),\quad y_{ref}^*(t)=y_{ref}\left(\frac{Nt}{2\omega_e}\right),\quad \omega_{ref}^*(t)=\omega_{ref}\left(\frac{Nt}{2\omega_e}\right) \tag{B.3a}$$

This readily implies that y_{ref}^* and ω_{ref}^* are in turn constant or periodic, with period 2π, and:

$$y_{ref}(t)=y_{ref}^*(2\tau/N),\quad \omega_{ref}(t)=\omega_{ref}^*(2\tau/N) \tag{B.3b}$$

Also, it is easily seen that $\dot W(\tau)=dW(\tau)/d\tau=\varepsilon dZ(t)/dt=\varepsilon\dot Z(t)$ with $\varepsilon=1/\omega_e$. Then, it follows from (51) that the state vector W undergoes the following state equation:

$$\dot W = \varepsilon AW + \varepsilon f_1(W,\tau,\varepsilon) + \varepsilon g\sigma_1(W_2,\tau,\varepsilon) + \varepsilon\varphi_0^T W + \varepsilon\Phi_0\Delta + h\dot y_{ref}^*(2\tau/N)\ \text{(using B.3b)} \tag{B.4a}$$

with

$$f_0(W,\tau,\varepsilon)=f(W,\varepsilon\tau),\quad \sigma_0(W_2,\tau,\varepsilon)=\sigma(W_2,\varepsilon\tau) \tag{B.4b}$$

$$\varphi_0(W_2,\tau,\varepsilon)=\varphi(W_2,\varepsilon\tau),\quad \Phi_0(W_2,\tau,\varepsilon)=\Phi(W_2,\varepsilon\tau) \tag{B.4c}$$

It readily follows from (50d) that

$$f_0(W,\tau,\varepsilon)=[\,0\quad \left(a_0k\cos(2\tau)+a_2w_1\cos(\tau)\right)\quad 0\,]^T \tag{B.4d}$$

where the following notations are adopted in coherence with (50a):

$$W=\begin{bmatrix}W_1\\W_2\end{bmatrix},\quad W_1=[\,w_1\quad w_2\quad w\,]^T,\quad W_2=[\,w_3\quad w_4\quad w_5\,]^T \tag{B.5}$$

According to system averaging theory, one gets stability results regarding the system of interest (B.4a)–(B.4b) by analyzing the averaged system defined by

$$\dot{\overline{W}} = \varepsilon A\overline{W} + \varepsilon\overline{f}_0(\overline{W}) + \varepsilon g\overline{\sigma}_0(\overline{W}_2) + \varepsilon\overline{\varphi}_0^T\overline{W} + \varepsilon\overline{\Phi}_0\Delta \quad \text{where } \overline{W}\in IR^6 \tag{B.6a}$$

with

$$\overline{f}_0(\overline{W}) \stackrel{def}{=} \lim_{\varepsilon\to 0}\frac{1}{2\pi N}\int_0^{2\pi N} f_1(\overline{W},\tau,\varepsilon)\,d\tau \tag{B.6b}$$

$$\overline{\sigma}_0(\overline{W}_2) \stackrel{def}{=} \lim_{\varepsilon\to 0}\frac{1}{2\pi N}\int_0^{2\pi N} \sigma_1(\overline{W},\tau,\varepsilon)\,d\tau \tag{B.6c}$$

$$\overline{\varphi}_0(\overline{W}) \stackrel{def}{=} \lim_{\varepsilon\to 0}\frac{1}{2\pi N}\int_0^{2\pi N} \varphi_0(\overline{W},\tau,\varepsilon)\,d\tau \tag{B.6d}$$

$$\overline{\Phi}_0(\overline{W}) \stackrel{def}{=} \lim_{\varepsilon\to 0}\frac{1}{2\pi N}\int_0^{2\pi N} \Phi_0(\overline{W},\tau,\varepsilon)\,d\tau \tag{B.6e}$$

Note that the last term on the right side of (48a) has not been accounted for in (B.6a) because its average value is null, due to the

periodicity (with period 2π) of y^*_{ref}. From (B.6c), one has

$$\overline{f}_0(\overline{W}) = [0 \quad 0 \quad 0]^T \tag{B.7}$$

In view of (B.7) the average system (B.6a) simplifies to

$$\dot{\overline{W}} = \varepsilon A\overline{W} + \varepsilon g\overline{\sigma}_0(\overline{W}_2) + \varepsilon\overline{\varphi}_0^T\overline{W} + \varepsilon\overline{\Phi}_0\Delta \tag{B.8}$$

where the following notations are used in coherence with (B.5) and (50a):

$$\overline{W} = \begin{bmatrix} \overline{W}_1 \\ \overline{W}_2 \end{bmatrix}, \quad \overline{W}_1 = \begin{bmatrix} \overline{w}_1 & \overline{w}_2 & \overline{w} \end{bmatrix}^T, \quad \overline{W}_2 = \begin{bmatrix} \overline{w}_3 & \overline{w}_4 & \overline{w}_5 \end{bmatrix}^T \tag{B.9}$$

In view of (50e) and (50h)–(50i) the vectors g, $\overline{\varphi}_0$ and $\overline{\Phi}_0$ assume the following partitions:

$$g = \begin{bmatrix} g_1 \\ 0_3 \end{bmatrix}, \quad \overline{\varphi}_0 = \begin{bmatrix} 0_3 \\ \overline{\varphi}_{01} \end{bmatrix}, \quad \overline{\Phi}_0 = \begin{bmatrix} 0_{3\times 3} \\ \overline{\Phi}_{01} \end{bmatrix} \tag{B.10a}$$

with

$$g_1 = \begin{bmatrix} 0 & \dfrac{-3}{2C} & a_3 \end{bmatrix}^T, \quad \overline{\varphi}_{01} = \begin{bmatrix} -k_1|\overline{\varphi}_1|^2 & -k_2|\overline{\varphi}_2|^2 & 0 \end{bmatrix}^T,$$
$$\overline{\Phi}_{01} = \begin{bmatrix} \overline{\varphi}_1 & \overline{\varphi}_2 & 0_3 \end{bmatrix}^T \tag{B.10b}$$

This together with (50c) implies that (B.8) can be decomposed in the following two state equations:

$$\dot{\overline{W}}_1 = \varepsilon A_1\overline{W}_1 + \varepsilon g_1\overline{\sigma}_0(\overline{W}_2) \tag{B.11a}$$

$$\dot{\overline{W}}_2 = \varepsilon A_2\overline{W}_2 + \varepsilon\overline{\varphi}_{01}^T\overline{W}_2 + \varepsilon\overline{\Phi}_{01}\Delta \tag{B.11b}$$

It is readily checked that the right side of the subsystem (B.11b) is nothing other than the right side of (49a)–(49b) multiplied by the positive coefficient ε. Such multiplication preserves the stability properties of (49a)–(49b). Therefore, it follows from Theorem 1 (Part 3) that the origin $[0\,0\,0]^T$ is an exponentially stable equilibrium of the system (B.11b) and, consequently,

$$\lim_{t\to\infty}\overline{W}_2(t) = 0, \text{ exponentially and whatever the initial value } \overline{W}_2(0) \tag{B.12}$$

Using again the fact that v_{dcref} and ω_{ref}, as well as their derivatives, are periodic (with period $N\pi/\omega_e$), it follows from (50g) and (B.6c) that $\overline{\sigma}_0(\overline{W}_2)$ is a polynomial function of $\overline{W}_2$. Then, (B.12) implies that

$$\lim_{t\to\infty}\overline{\sigma}_0(\overline{W}_2(t)) \approx \overline{\sigma}_0(0_3), \text{ exponentially and whatever } \overline{W}_2(0) \tag{B.13}$$

Now, let us check that A_1 is in turn Hurwitz. Its characteristic polynomial is

$$\det(\lambda I - A_1) = \lambda^3 + (c_1+b)\lambda^2 + b(c_1+c_2)\lambda + bc_1c_2 \tag{B.14}$$

Applying for instance the well known Routh's algebraic criteria, it follows that all zeros of the polynomial (B.14) have negative real parts if the coefficients c_1,c_2 and b are positive which actually is the case. Hence, the matrix A_1 is Hurwitz implying that the autonomous part of the linear system (B.11a) is globally exponentially stable. Then, one gets from (B.13) that the solution of the nonautonomous system (B.11a) satisfies:

$$\lim_{t\to\infty}\overline{W}_1(t) = \overline{\sigma}_0(0_3)A_1^{-1}g_1, \text{ exponentially and whatever } \overline{W}_1(0). \tag{B.15}$$

Notice the exponential feature of the convergence is due to the linearity of (B.11a). Combining (B.13) and (B.14), it follows that state vector

$$W^* \overset{def}{=} \begin{bmatrix} \overline{\sigma}_0(0_3)A_1^{-1}g_1 \\ 0_3 \end{bmatrix} \in IR^6 \tag{B.15}$$

is a globally exponentially stable equilibrium of the average system (B.8). Now, invoking the averaging theory, e.g. Theorem 10.4 in Khalil (2003), it follows that there exists a positive real constants ε^* such that, if $0<\varepsilon<\varepsilon^*$ then, the differential equation (B.4a) has a 2π-periodic solution $W(\tau)=W(\tau,\varepsilon)$, that continuously depends on ε and that

$$\lim_{\varepsilon\to 0} W(\tau,\varepsilon) = W^* \tag{B.16a}$$

The same result applies to the original differential equation (B.2) using the relation $Z(t)=W(\tau)$ with $\tau=\omega_e t$. That is, $Z(t)=Z(t,\varepsilon)$ is $(2\pi/\omega_e)$-periodic, it depends continuously on ε and:

$$\lim_{\varepsilon\to 0} Z(\tau,\varepsilon) = W^* \tag{B.16b}$$

This establishes Part 2-a of Theorem 2. To prove Part 2-b, let us obtain more insight on the equilibrium W^*. In coherence with (50a), this is decomposed as follows:

$$W^* = \begin{bmatrix} W_1^* \\ W_2^* \end{bmatrix}, \quad W_1^* = \begin{bmatrix} w_1^* & w_2^* & w^* \end{bmatrix}^T, \quad W_2^* = \begin{bmatrix} w_3^* & w_4^* & w_5^* \end{bmatrix}^T \tag{B.17}$$

Then, it readily follows from (B.15) that

$$W_1^* = \overline{\sigma}_1(0_3)A_1^{-1}g_1 \text{ and } W_2^* = 0_3 \tag{B.18a}$$

Also, it is readily checked using (50c) and (B.10) that

$$W_1^* = \overline{\sigma}_1(0_3)A_1^{-1}g_1 = \overline{\sigma}_1(0_3)\begin{bmatrix} 0 & \dfrac{3b-2Ca_0a_3}{2Ca_0a_1} & \dfrac{-3}{2Ca_0} \end{bmatrix}^T \tag{B.18b}$$

Furthermore, it is obviously seen from (50b) that

$$\frac{3b-2Ca_0a_3}{2Ca_0a_1} = 0 \tag{B.18c}$$

Consequently, one gets from (B.16b), (B.17), (B.18b) and (B.18c) that

$$\lim_{\varepsilon\to 0} z_2(t,\varepsilon) = w_2^* = 0 \tag{B.19a}$$

$$\lim_{\varepsilon\to 0} k(t,\varepsilon) = w^* = -\frac{3\overline{\sigma}_1(0_3)}{2Ca_0} \tag{B.19b}$$

Finally, notice that

$$\begin{aligned}\overline{\sigma}_0(0_3) &= \lim_{\varepsilon\to 0}\frac{1}{2\pi N}\int_0^{2\pi N}\sigma_0(0_3,\tau,\varepsilon)\,d\tau \quad \text{(using (B.6c))} \\ &= \lim_{\varepsilon\to 0}\frac{1}{2\pi N}\int_0^{2\pi N}\sigma(0_3,\varepsilon\tau)\,d\tau \quad \text{(using (B.4b))}\end{aligned} \tag{B.20a}$$

Introducing the variable change $\tau=\omega_e t$, (B.20a) becomes

$$\overline{\sigma}_0(0_3) = \lim_{\varepsilon\to 0}\frac{\omega_e}{2\pi N}\int_0^{2\pi N/\omega_e}\sigma(0_3,t)\,dt = \overline{\sigma}(0_3) \tag{B.20b}$$

This, together with (B.19a)–(B.19b), establishes Part 2-b.

Part 3: It has already been noticed that the stability properties of (B.11b) are identical to those of (49a)–(49b). Therefore, it follows using Theorem 1 (Part 2) that the vector $\overline{W}_2(t)$ converges exponentially to a compact neighborhood of the origin $[0\,0\,0]^T$ and the size of this compact is inversely proportional to $c\kappa$ and so can be made arbitrarily small by letting $\kappa = \min(k_1,k_2)$ and $c = \min(c_3,c_4,c_5)$ be sufficiently large. Then, following closely the proof of Part 2 (starting immediately after Eq. (B.12)), it can be readily checked that all equations from (B.13) to (B.20b) still hold with an error that is inversely proportional to $c\kappa$. This establishes Part 3 and completes the proof of Theorem 2.

References

Elmas, C., & Ustun, O. (2008). A hybrid controller for the speed control of a permanent magnet synchronous motor drive. *Control Engineering Practice*, *16*(3), 260–270.

Khalil, H. (2003). *Nonlinear systems*. NJ, USA: Prentice Hall.

Krstic, M., Kanellakopoulos, I., & Kokotovic, P. (1995). *Nonlinear and adaptive control design*. John Wiley & Sons, Inc.

Kuroe, Y., Okamura, K., Nishidai, H., & Maruhashi, T. (1998). Optimal speed control of synchronous motors based on feedback linearization. In International conference on power electronics and variable-speed drives (pp. 328–331). London, UK.

Michael, J., Ryan, D., & Rik, W. (1998). Modeling of sinewave inverters: a geometric approach. In The annual conference of the IEEE industrial electronics society (IECON) (Vol. 1, pp. 396–401).

Muhammad, H., & Rashid, H. (2001). *Power electronics handbook*. Academic Press.

Pyrhonen, O., Niemela, M., Pyrhonen, J., & Kaukonen, J. (1998). Excitation control of DTC controlled salient pole synchronous motor in field weakening range. In International workshop on advanced motion control, AMC '98 (pp. 294–298). Coimbra.

Saleh, K. I., Mohammed, O. A., & Badr, M. A. (2004). Field oriented vector control of synchronous motors with additional field winding. *IEEE Transactions on Energy Conversion*, *19*, 95–101.

Singh, B., Bhuvaneswari, G., & Garg, V. (2006). Improved power quality AC–DC converter for electric multiple units in electric traction. In IEEE Power India Conference (p. 6).

Sira, H., & Silva, R. (2006). *Control design techniques in power electronics devices*. Springer.

Wallmark, O. (2004). On control of permanent-magnet synchronous motors in hybrid-electric vehicle application. Technical report, School of Electrical Engineering, Chalmers University of technology Goteborg, Sweden.

Yang, Z. P., Wang, M. H., Liu, C. L., Hou, C. L., & Cai, Y. B. (1992). Variable structure control with sliding mode for self-controlled synchronous motor drive speed regulation. *IEEE International Symposium on Industrial Electronics (ISIE)*, *2*, 620–624.